Hyperfine Interact (2016) 237:75
DOI 10.1007/s10751-016-1258-9

^{57}Fe emission Mössbauer spectroscopy following dilute implantation of ^{57}Mn into In_2O_3

A. Mokhles Gerami[1,2] · K. Johnston[1,3] · H. P. Gunnlaugsson[1] · K. Nomura[4] · R. Mantovan[5] · H. Masenda[6] · Y. A. Matveyev[7] · T. E. Mølholt[1] · M. Ncube[6] · S. Shayestehaminzadeh[8] · I. Unzueta[9] · H. P. Gislason[8] · P. B. Krastev[10] · G. Langouche[11] · D. Naidoo[6] · S. Ólafsson[8] · the ISOLDE collaboration[1]

© Springer International Publishing Switzerland 2016

Abstract Emission Mössbauer spectroscopy has been utilised to characterize dilute ^{57}Fe impurities in In_2O_3 following implantation of ^{57}Mn ($T_{1/2}$ = 1.5 min.) at the ISOLDE

This article is part of the Topical Collection on *Proceedings of the International Conference on the Applications of the Mössbauer Effect (ICAME 2015), Hamburg, Germany, 13–18 September 2015*

✉ H. P. Gunnlaugsson
Haraldur.p.gunnlaugsson@cern.ch

1 CERN, PH Div, 1211 Geneve 23, Switzerland

2 Department of physics, K.N.Toosi University of Technology, P.O.Box 15875-4416, Tehran, Iran

3 Universität des Saarlandes, Experimentalphysik, 66123 Saarbrucken, Germany

4 Photocatalysis International Research Center, Tokyo University of Science, Yamazaki 2641, Noda, 278-8501, Japan

5 Laboratorio MDM, IMM-CNR, Via Olivetti 2, 20864 Agrate Brianza (MB), Italy

6 School of Physics, University of the Witwatersrand, Witwatersrand, South Africa

7 Moscow Institute of Physics and Technology, 9 Institutskiy per., Dolgoprudny, Moscow Region, 141700, Russian Federation

8 Science Institute, University of Iceland, Dunhaga 3, IS-107 Reykjavík, Iceland

9 BCMaterials & Elektrizitate eta Elektronika Saila, Euskal Herriko Unibertsitatea (UPV/EHU), 48048 Bilbao, Spain

10 Institute for Nuclear Research and Nuclear Energy, Bulgarian Academy of Sciences, 72 Tsarigradsko Chaussee Boulevard, Sofia, 1784, Bulgaria

11 KU Leuven, Instituut voor Kern-en Stralings Fysika, Leuven, Belgium

Published online: 02 March 2016

facility at CERN. From stoichiometry considerations, one would expect Fe to adopt the valence state 3+, substituting In^{3+}, however the spectra are dominated by spectral lines due to paramagnetic Fe^{2+}. Using first principle calculations in the framework of density functional theory (DFT), the density of states of dilute Fe and the hyperfine parameters have been determined. The hybridization between the 3d-band of Fe and the 2p band of oxygen induces a spin-polarized hole on the O site close to the Fe site, which is found to be the cause of the Fe^{2+} state in In_2O_3. Comparison of experimental data to calculated hyperfine parameters suggests that Fe predominantly enters the 8b site rather than the 24d site of the cation site in the Bixbyite structure of In_2O_3. A gradual transition from an amorphous to a crystalline state is observed with increasing implantation/annealing temperature.

Keywords In_2O_3 · Fe doping · ^{57}Mn implantation · Emission Mössbauer spectroscopy · Annealing · Density functional theory

1 Introduction

Doping non-magnetic semiconductors with 3d-elements to obtain dilute magnetic semiconductors (DMSs) has motivated a large amount of research following the theoretical prediction of room temperature (RT) ferromagnetism in ZnO-based DMSs [1]. Here Fe doped In_2O_3 is among the systems where DMS has been reported [2], and where the charge state of Fe has been suggested to play an important role in the magnetic properties [3, 4].

In_2O_3 is a wide bandgap semiconductor, and is of interest due to its good electrical conductivity and high optical transparency [5]. Crystalline In_2O_3 has a body-centred cubic structure known as Bixbyite (space group Ia-3 (206)). There are two different kinds of cation sites, denoted as 24d and 8b, and the ratio of 24d and 8b sites in a unit cell is 3:1 [6–8]. The 8b cation site has octahedral symmetry and is surrounded by 6 equivalent nearest neighbour oxygen atoms. The 24d cation site has asymmetric structure and is surrounded by 6 neighbour oxygen atoms with three pairs distances ($d_1 < d_2 < d_3$) (Fig. 1b). These sites have been proposed to have different magnetic states [9–12].

In order to investigate the site occupancy and chemical or magnetic properties of dilute Fe in ion-implanted In_2O_3, we have performed ^{57}Fe emission Mössbauer Spectroscopy (eMS) following implantation of radioactive ^{57}Mn ($T_{1/2} = 1.5$ min.) at the ISOLDE facility at CERN. The results are compared to calculations using density functional theory (DFT) within the Wien2K package [13, 14].

2 Experimental methods and samples

Beams of ^{57}Mn ($T_{1/2} = 1,5$ min.) were produced at the ISOLDE/CERN by 1.4 GeV proton induced fission in a heated UC_x target. Element selective laser ionization was used to ionize manganese, which was then accelerated to 50 keV. After magnet mass separation, a clean beam with intensity of few times 10^8 $^{57}Mn^+$/s was obtained. The ^{57}Mn ions were implanted into In_2O_3 polycrystalline films with columnar structure heated from the backside with a halogen lamp inside an implantation chamber. Implantation took place at 30° relative to the sample surface normal. Emission Mössbauer spectra were measured at 60° relative to the sample surface normal with a Parallel Plate Avalanche Detector (PPAD) equipped with ^{57}Fe-enriched stainless steel mounted on a conventional drive system outside the implantation chamber. The implantation fluence rate was $\sim 10^9$ ^{57}Mn/(cm^2· s) and

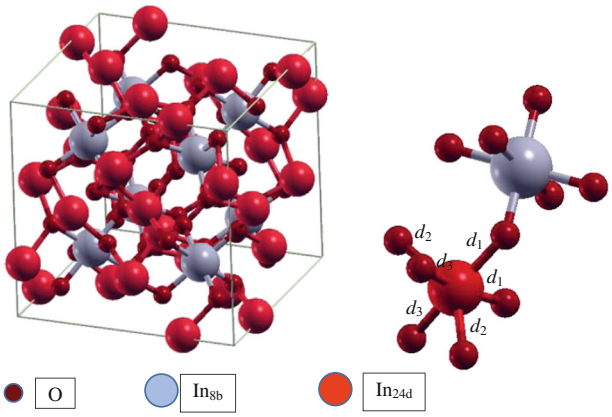

Fig. 1 Crystalline structure of In_2O_3. *Left*: Big spheres are the two different In sites and small spheres are O anions. *Right*: the crystallographic view of the two In sites

the maximum fluence per sample was $\sim 10^{12}$ ^{57}Mn/cm^2, corresponding to a maximum concentration of 4×10^{-4} at.%. Isomer shifts and velocities are given relative to the centre of the α-Fe spectrum at RT.

3 Computational method

Using the WIEN2K code [13], the isomer shift (δ) and quadrupole splitting (ΔE_Q) parameters have been calculated within density functional theory by considering the generalized gradient approximation (GGA) [14]. The Pedrew Burke Ernzerhof (PBE) of GGA functional was used for all of the DFT calculations [15]. In the calculations performed, the radii of the muffin-tin atomic spheres of In, O, and Fe are set to 2.15, 1.8, and 2.10 a.u., respectively. In addition, the energy value of -6 Ry is set as the boundary separating the core electron states and valence electron states. The cut-off parameter $R_{MT}K_{MAX}$, which controls the size of the basis set, is set to 7.0, a mesh of $(4 \times 4 \times 4)$ k-points in the irreducible part of the first Brillouin zone was applied to the self-consistent total energy calculation. Within this approach, the calculations of the Fe-doped In_2O_3 in different configurations were performed with the lattice constant of virgin In_2O_3 at room temperature, based on a periodic supercell of 80 atoms.

The isomer shift is obtained from the contact densities (ρ) as [16]:

$$\delta = \alpha(\rho_A - \rho_s) \tag{1}$$

where, ρ_A and ρ_s are the charge densities at the nucleus in the absorber (A) and sample (S) material, respectively. The calibration constant of $\alpha = -0.29$ a.u.^{3} mm/s as in Ref. [17] was used. The electric field gradient tensor (EFG), expressed by its principal component (V_{ZZ}) and the asymmetry parameter (η) gives the quadrupole splitting as

$$\Delta E_Q = \frac{eQV_{ZZ}}{2}\sqrt{1 + \eta^2/3} \tag{2}$$

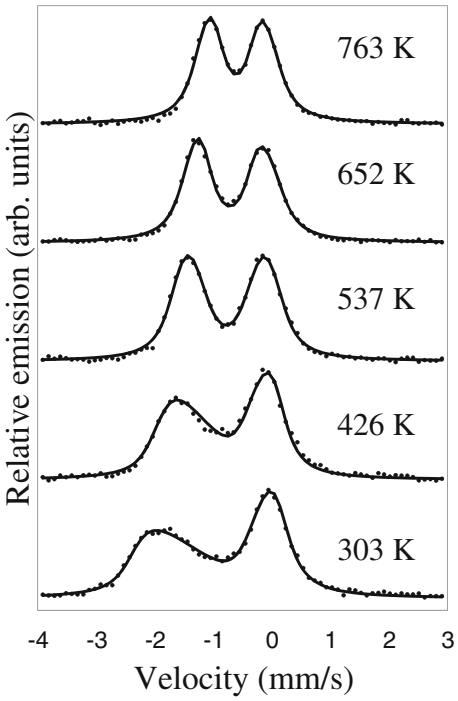

Fig. 2 ^{57}Fe emission Mössbauer spectra obtained after implantation of ^{57}Mn into In_2O_3 sample held at the temperatures indicated

where e is the elementary charge and $Q = 0.16 \cdot 10^{-28}$ m^2 [18] is the nuclear quadrupole moment of the 14.4 keV Mössbauer state of ^{57}Fe.

4 Experimental results

The eMS spectra obtained (Fig. 2) are dominated by a single asymmetric quadrupole split component with isomer shift characteristic of high spin Fe^{2+}. The spectra were analysed using the program Vinda [19] with a quadrupole splitting distribution where the distribution function was simulated with two linear segments [20]. To account for the asymmetry, a coupling between isomer shift and quadrupole splitting was assumed as $\delta = d_0 + d_1 \cdot \Delta E_Q$, where d_0 and d_1 are fitting variables. As seen in the fit in Fig. 2, this model adequately explains the experimental data although the spectrum obtained at 426 K could benefit from a more complicated (3 segment) distribution function. At room temperature, there are noticeable signs of a misfit due to a broad Fe^{3+} component. Figure 3 shows a zoom-in of the spectral intensity close to the background in the 300 K measurement.

There is a small, but significant tail around $v \sim 4$ and -8 mm/s, which the quadrupole splitting distribution cannot describe. A plausible explanation for this would be high spin Fe^{3+} showing slow paramagnetic relaxations, as observed in other oxides in similar experiments [21–23]. Such a feature could account for ∼6 % of the relative spectral area. At temperatures >426 K, this feature has disappeared completely from the spectra.

The isomer shift (Fig. 4a) clearly identifies the doublet component as due to high-spin Fe^{2+}. There is a change of trend on how the experimental data follows the second order Doppler shift, suggesting an annealing stage between 400 and 500 K. The average

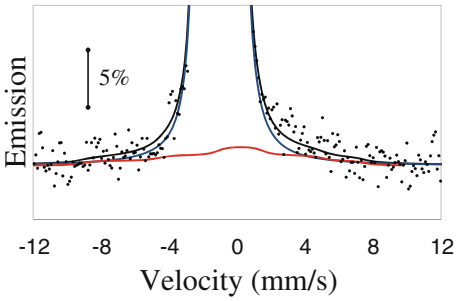

Fig. 3 Spectral intensity close to the baseline in the 300 K spectrum. The peak of the spectrum is at 220 % above the background

quadrupole splitting (Fig. 4b) shows a gradual decrease through the temperature range as expected for a temperature-dependent population of 3d orbitals. The width of the quadrupole splitting distribution represented by its standard deviation (Fig. 4c) also shows a change between 400 and 500 K, again suggesting a change in the nature of the Fe sites, as was observed with the trend of the isomer shift (Fig. 4a). The coupling between isomer shift and quadrupole splitting (Fig. 4d) shows a complicated dependence. Below 500 K it is negative, peaks with a positive value at ∼650 K and then decreases again.

5 Theoretical results

The hyperfine parameters and the local structure around the Fe probe in In_2O_3 were simulated using first principle calculations for Fe on two different In sites with a dilution of 1:32 which corresponds to concentration of 3.12 %, the octahedrons of Fe at 8b site and the distorted octahedrons of Fe at 24d site as illustrated in Fig. 1. The density of states (DOSs) of the two calculated configurations are presented in Fig. 5. The valence band of In_2O_3 is mainly composed of 2p oxygen states, while the conduction band is mainly composed of 4s In states. By doping Fe on the In_{8b} site in In_2O_3, the 3d energy levels are split into three- and two-fold degenerate $t_{2g}(d_{xy}, d_{xz}, d_{zy})$ and e_g-levels $(d_{z^2}, d_{x^2-y^2})$ with the t_{2g} levels lower in energy (Fig. 5b). Four electrons are in t_{2g} ($3t_{2g}\uparrow$,$1t_{2g}\downarrow$) level energy and two electrons are in e_g ($2e_g\uparrow$) level energy. From Fig. 5b and d, it is seen that the energy level of 3d states are merged with the valence band. This causes hybridization between the 3d and 2p states. This hybridization creates spin polarized hole states on the oxygen sites. Since, the 3d band of Fe ions is more than half filled, the spin on the hole state of the oxygen sites will be parallel to the spin of Fe ions. These findings are in accordance with the findings of Huang et al. [7]. Therefore, we expect the charge state of Fe substituting the In^{3+}site to be close to 2+. This calculation is in agreement with the measured eMS data, which show Fe in the high spin 2+ state. Due to the presence of asymmetry at the Fe_{24d} site, the d levels of energy for Fe get split to three energy levels $(d_{z^2}, d_{x^2-y^2} + d_{xy}, d_{xz} + d_{yz})$ (Fig. 5d). The calculated hyperfine parameters are given in Table 1.

6 Discussion

A simple explanation of the temperature-dependence of the hyperfine parameters (Fig. 4) is in terms of the annealing of local implantation-induced amorphous zones between 400 K

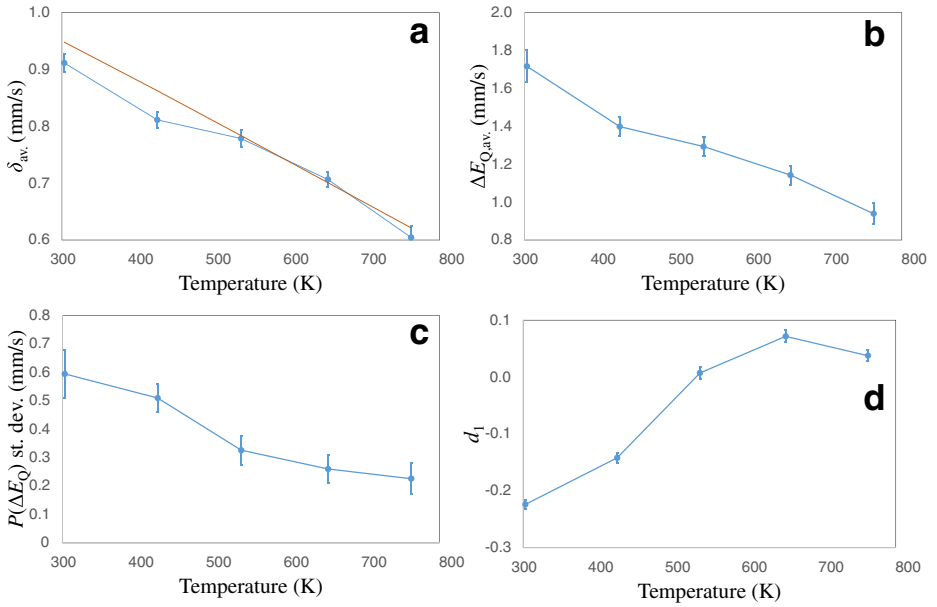

Fig. 4 Temperature dependence of hyperfine parameters obtained from the analysis of the eMS spectra in Fig. 2. **a** Isomer shift compared to the second order Doppler shift (SOD). **b** Average quadrupole splitting. **c** Standard deviation of the quadrupole splitting distribution **d** The coupling parameter between quadrupole splitting and isomer shift

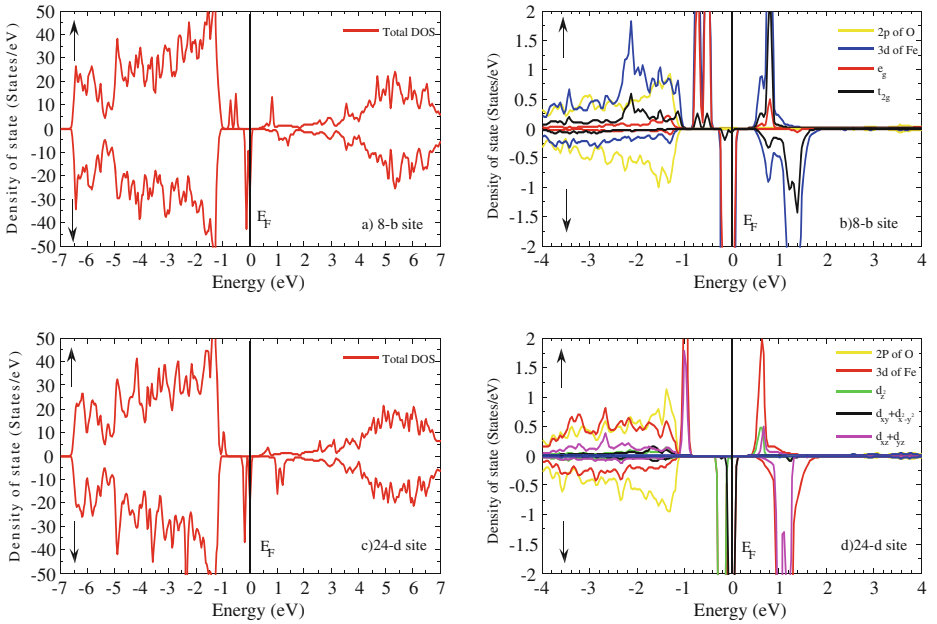

Fig. 5 Projected DOSs of the total structure of $In_{1-x}Fe_xO$ for **a**) 8b site of Fe and **c**) 24d site of Fe and the contribution of Fe and O orbitals are plotted of the **b**) 8b site and **d**) 24d site

Table 1 DFT calculated nuclear hyperfine parameters for Fe on the two different sites of In in In_2O_3, as indicated in the symmetry structure

Position of Fe	$V_{ZZ}(\times 10^{21}$ V/m$^2)$	δ(mm/s)	ΔE_Q(mm/s)	Mössbauer spectroscopy Line
Fe_{8b}	6.3	0.81	1.06	Fe^{2+} in crystalline phase
Fe_{24d}	3.06	0.82	0.51	

and 500 K. This would explain the change in isomer shift (Fig. 4a) and width of the quadrupole splitting distribution (Fig. 4c). The data then suggests that Fe^{2+} in amorphous zones is characterized by a negative coupling between isomer shift and quadrupole splitting, whereas the crystalline environment is characterized by a positive coupling (Fig. 4d). The two cation sites in the Bixbyite structure suggest that in the crystalline environment, one should observe two quadrupole doublets (if both sites are populated) and this could be the source of a positive coupling between the isomer shift and quadrupole splitting around 650 K. Alternatively, nearby defects can affect both the isomer shift and quadrupole splitting, giving an alternative explanation of these features.

The calculated hyperfine parameters for Fe on the 8b site in In_2O_3 (Table 1) are in reasonable agreement with the experimental hyperfine parameters (Fig. 4), as extrapolated from the crystalline phase. By comparing the experimental data with the DFT calculations, we can conclude that the fraction of Fe atoms at the 8b site is larger than at the 24d site.

It is noteworthy to add that a spectral component related to interstitial Fe, which could be expected because of the $\langle E_R \rangle \approx 40$ eV recoil imparted on the ^{57}Fe daughter in the β^- decay of ^{57}Mn, is not observed. A possible explanation is that the threshold displacement energy is too high ($\sim$90 eV), but this seems to be at variance with the results of Walsh et al. [24] which based on theoretical calculations predicted threshold displacement energy of 14.2 eV. Alternatively, the Debye-Waller factor of interstitial Fe is too low to allow for the detection of interstitial Fe or that interstitial Fe is incorporated on In sites much faster than the lifetime of the Mössbauer state (140 ns).

The hyperfine parameters obtained here differ significantly from the parameters reported by Yan et al. [3] who used sol-gel In_2O_3 material with a $\sim$15 % Fe doping, showing two Fe^{3+} doublets assigned to Fe on 8b sites and 24d sites. After annealing in vacuum, the Fe^{3+} doublet due to Fe on 24d sites disappeared, and a magnetic sextet due to Fe^{2+} appeared in the spectrum assigned to Fe^{2+} on 24d sites stabilized by the introduction of oxygen vacancies in the annealing process [3].

It is difficult to see any correlation between our results and the results of [3], and the different concentration of Fe and/or sample material must be the explanation for the very different findings. Yang et al. [4] found both Fe^{2+} and Fe^{3+} in $<$16 % Fe doped In_2O_3 samples prepared by magnetron sputtering, suggesting a transformation from the dilute case where Fe^{2+} dominates to a Fe^{3+} dominating state, depending on the Fe concentration. This seems though to be at variance with the results of Nomura et al. which saw only doublets due to Fe^{3+} in sol-gel indium tin oxide material with 6 % Fe [25].

It should be noted, that the results of the calculations presented here differ from those of Ref. [26]. One possible reason is that in the calculations of Ref. [26] one Fe per half unit cell is considered, while in the present calculations one Fe per unit cell is considered. The splitting observed in our calculations, is closer to predictions of crystal field theory of the local symmetry (twofold splitting in 8b symmetry and threefold splitting in 24d symmetry), giving us confidence to the current calculations.

7 Conclusions

^{57}Fe Emission Mössbauer spectroscopy following dilute implantation of ^{57}Mn shows an annealing stage at 400–500 K. Above this annealing stage, the Fe probe atoms are incorporated on regular substitutional In lattice sites. The experimental data show that Fe^{2+} replaces In^{3+}. With the spin of Fe parallel with the spin of the hole state on oxygen orbital which is due to strong hybridization between the 3d orbitals of Fe and the 2p orbitals of O, the density functional theory calculations suggest Fe^{2+} state in In_2O_3. Furthermore, the calculated hyperfine parameters are in reasonable agreement with Fe^{2+} predominantly incorporated on the 8b site of the Byxibite In_2O_3 structure.

Acknowledgments This work was supported by the European Union Seventh Framework through ENSAR (Contract No. 262010). R. Mantovan acknowledges support from MIUR through the FIRB Project RBAP115AYN "Oxides at the nanoscale: multifunctionality and applications." H. Masenda, D. Naidoo, and M. Ncube acknowledge support from the South African National Research Foundation and the Department of Science and Technology. T. E. Mølholt, H. P. Gislason, and S. Ólafsson acknowledge support from the Icelandic Research Fund (Grant No. 110017021-23). Unzueta acknowledge financial support from Basque Government Grants nos. IT-443-10 and PRE_2014_214.

References

1. Dietl, T., Ohno, H., Matsukura, F., Cibert, J., Ferrand, D.: Zener model description of ferromagnetism in Zinc-Blende magnetic semiconductors. Science **287**, 1019–1022 (2000). doi:10.1126/science.287.5455.1019
2. He, J., Xu, S., Yoo, Y.K., Xue, Q., Lee, H.-C., Cheng, S., Xiang, X.D., Dionne, G.F., Takeuchi, I.: Room temperature ferromagnetic n -type semiconductor in $(In_{1-x}Fe_x)_2O_{3-\sigma}$. Appl. Phys. Lett. **86**, 052503 (2005). doi:10.1063/1.1851618
3. Yan, S., Qiao, W., Zhong, W., Au, C.-T., Dou, Y.: Effects of site occupancy and valence state of Fe ions on ferromagnetism in Fe-doped In_2O_3 diluted magnetic semiconductor. Appl. Phys. Lett. **104**, 062404 (2014). doi:10.1063/1.4865102
4. Yang, D., Feng, D., Wu, Z., Ma, G., Liu, J., An, Y.: Structure, optical and magnetic properties of $(In_{1-x}Fe_x)_2O_3$ films by magnetron sputtering. J. Alloy. Compd. **619**, 869–875 (2015). doi:10.1016/j.jallcom.2014.09.094
5. Bierwagen, O.: Indium oxide–a transparent, wide-band gap semiconductor for (opto)electronic applications. Semicond. Sci. Technol. **30**, 024001 (2015). doi:10.1088/0268-1242/30/2/024001
6. Hu, S.-j., Yan, S.-s., Lin, X.-l., Yao, X.-x., Chen, Y.-x., Liu, G.-l., Mei, L.-m.: Electronic structure of Fe-doped In_2O_3 magnetic semiconductor with oxygen vacancies: Evidence for F-center mediated exchange interaction. Appl. Phys. Lett. **91**, 262514 (2007). doi:10.1063/1.2828041
7. Huang, L.M., Moysés, C., Araújo, Ahuja, R.: Magnetic and electronic properties of 3d transition-metal-doped In_2O_3: an ab initio study. Europhys. Lett. **87**, 27013 (2009). doi:10.1209/0295-5075/87/27013
8. Qi, S., Jiang, F., Fan, J., Wu, H., Zhang, S.B., Gehring, G.A., Zhang, Z., Xu, X.: Carrier-mediated nonlocal ferromagnetic coupling between local magnetic polarons in Fe-doped In_2O_3 and Co-doped ZnO. Phys. Rev. B **205204**, 84 (2011). doi:10.1103/PhysRevB.84.205204
9. Kohiki, S., Sasaki, M., Murakawa, Y., Hori, K., Okada, K., Shimooka, H., Tajiri, T., Deguchi, H., Matsushima, S., Oku, M., Shishido, T., Arai, M., Mitome, M., Bando, Y.: Doping of Fe to In_2O_3. Thin Solid Films **505**, 122–125 (2006). doi:10.1016/j.tsf.2005.10.022
10. Xu, X.-H., Jiang, F.-X., Zhang, J., Fan, X.-C., Wu, H.-S., Gehring, G.A.: Magnetic and transport properties of n-type Fe-doped In_2O_3 ferromagnetic thin films. Appl. Phys. Lett. **212510**, 94 (2009). doi:10.1063/1.3147190
11. Jiang, F.-X., Xu, X.-H., Zhang, J., Fan, X.-C., Wu, H.-S., Alshammari, M., Feng, Q., Blythe, H.J., Score, D.S., Addison, K., Al-Qahtani, M., Gehring, G.A.: Room temperature ferromagnetism in metallic and insulating $(In_{1-x}Fe_x)_2O_3$ thin films. J. Appl. Phys. **109**, 053907 (2011). doi:10.1063/1.3559298
12. Tandon, B., Shanker, G.S., Nag, A.: Multifunctional Sn-, Fe-codoped In_2O_3 nanocrystals plasmonics and magnetism. J. Phys. Chems. Lett. **5**, 2306–2311 (2014). doi:10.1021/jz500949g

13. Blaha, P., Schwarz, K., Madsen, G.K.H., Kvasnicka, D., Luitz, J.: WIEN2k, an augmented plane wave + local orbitals program for calculating crystal properties, ISBN 3-9501031-1-2, Karlheinz Schwarz, Techn. Universität Wien, Austria (2001)
14. Perdew, J.P., Burke, K., Ernzerhof, M.: Generalized gradient approximation made simple. Physical Review Letters **77**, 3865 (1996). 10.1103/PhysRevLett.77.3865
15. Perdew, J.P., Chevary, J.A., Vosko, S.H., Pederson, M.R., Singh, D.J., Fiolhais C.: Atoms, molecules, solids, and surfaces: Applications of the generalized gradient approximation for exchange and correlation. Phys. Rev. B **46**, 6671 (1992). doi:10.1103/PhysRevB.46.6671
16. Neese, F.: Prediction and interpretation of the ^{57}7Fe isomer shift in Mössbauer spectra by density functional theory. Inorg. Chim. Acta **337**, 181–192 (2002). doi:10.1016/S0020-1693(02)01031-9
17. Wdowik, U.D., Ruebenbauer, K.: Calibration of the isomer shift for the 14.4 keV transition in ^{57}Fe using the full-potential linearized augmented plane-wave method. Phys. Rev. B **76**, 155118 (2007). doi:10.1103/PhysRevB.76.155118
18. Dufek, P., Blaha, P., Schwarz, K.: Determination of the nuclear quadrupole moment of ^{57}Fe. Phys. Rev. Lett. **75**, 3545–3548 (1995). doi:10.1103/PhysRevLett.75.3545
19. Gunnlaugsson, H.P.: Spreadsheet based analysis of Mössbauer spectra hyperfine interact. accepted (2015)
20. Gunnlaugsson, H.P.: A simple model to extract hyperfine interaction distributions from Mössbauer spectra. Hyperfine Interact **167**, 851–854 (2006). doi:10.1007/978-3-540-49853-724
21. Gunnlaugsson, H.P., Mantovan, R., Mølholt, T.E., Naidoo, D., Johnston, K., Masenda, H., Bharuth-Ram, K., Langouche, G., Ólafsson, S., Sielemann, R., Weyer, G., Kobayashi, Y.: the ISOLDE Collaboration: Mössbauer spectroscopy of ^{57}Fe in α-Al_2O_3 following implantation of ^{57}Mn*. Hyperfine Interact **198**, 5–14 (2010). doi:10.1007/s10751-010-0184-5
22. Mølholt, T.E., Mantovan, R., Gunnlaugsson, H.P., Naidoo, D., Ólafsson, S., Bharuth-Ram, K., Fanciulli, M., Johnston, K., Kobayashi, Y., Langouche, G., Masenda, H., Sielemann, R., Weyer, G., Gíslason, H.P.: Observation of spin-lattice relaxations of dilute Fe^{3+} in MgO by Mössbauer spectroscopy. Hyperfine Interact **197**, 89–94 (2010). doi:10.1007/s10751-010-0214-3
23. Mantovan, R., Gunnlaugsson, H.P., Johnston, K., Masenda, H., Mølholt, T.E., Naidoo, D., Ncube, M., Shayestehaminzadeh, S., Bharuth-Ram, K., Fanciulli, M., Gislason, H.P., Langouche, G., Ólafsson, S., Pereira, L.M.C., Wahl, U., Torelli, P., Weyer, G.: Atomic-scale magnetic properties of truly 3d-diluted ZnO. Adv. Electron. Mater. **1**, 1400039 (2015). doi:10.1002/aelm.201400039
24. Walsh, A., Woodley, S.M., Richard, C., Catlow, A., Sokol, A.A.: Potential energy landscapes for anion Frenkel-pair formation in ceria and India. Solid State Ionics **184**, 52–56 (2011). doi:10.1016/j.ssi.2010.08.010
25. Nomura, K., Sakuma, J., Ooki, T., Takeda, M.: Mössbauer study on indium tin oxides (ITO) doped with Fe. Hyperfine Interact **184**, 117–121 (2008). doi:10.1007/s10751-008-9775-9
26. Sena, C., Costa, M.S., Muñoz, E.L., Cabrera-Pasca, G.A., Pereira, L.F.D., Mestnik-Filho, J., Carbonari, A.W., Coaquira, J.A.H.: Charge distribution and hyperfine interactions in the vicinity of impurity sites in In_2O_3 doped with Fe, Co, and Ni. J. Magn. Magn. Mat. **387**, 165–178 (2015). doi:10.1016/j.jmmm.2015.03.092